Next-generation active integrated optic subsystems
Information society technologies programme
of the European Commission, project IST-2000-28018
Workpackage 3: Design

— Confidential, NAIS internal document. —

Coupled mode model for 3D directional couplers

Contents

Concepts and ideas in this draft originate from contributions from several participants in the NAIS project.

Contact: Manfred Hammer,
Faculty of Mathematical Sciences, University of Twente, P.O. Box 217, 7500 AE Enschede, The Netherlands
Phone: +31/53/489-3448, Fax: +31/53/489-4833, E-mail: m.hammer@math.utwente.nl

1 Adiabatic directional couplers, coupled mode viewpoint

A common model for optical ringresonators [1, 2] relies crucially upon an adequate description of the coupling regions between the cavity and the port channels. Figure 1 shows a sketch of that coupling region for a cylindrical cavity.

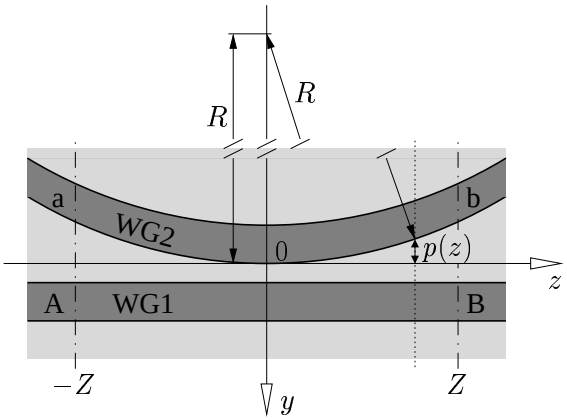

Figure 1: Top view of the directional coupler configuration: A segment of a cylindrical waveguide core (WG2) with radius R, evanescently coupled to a straight waveguide (WG1). Letters A, B, a, b denote the port positions of the device, p is the local y-displacement of the ring rim at position z.

The z-axis indicates the dominant direction of light propagation, with the origin positioned such that the arrangement is symmetric with respect to the plane $z = 0$. The lateral y-axis is oriented along a radius of the ring; $y = 0$ marks the outer rim of the ring at $z = 0$. At position z, this outer rim is shifted to $y = -p(z)$ with $p(z) = R - \sqrt{R^2 - z^2}$. Note that in general a threedimensional configuration is considered, i.e. the port core may be placed underneath the ring waveguide (see e.g. the cross section of Figure 2).

For a large ring radius, the structure can be treated by means of more or less standard coupled mode theory [3]:

- The optical electromagnetic field is represented by the two single guided modes of proper polarization that are supported by the isolated cores of the port and the ring waveguide. For the present simulations, the bend modes of the curved cavity waveguide are replaced by fields calculated for a *straight* waveguide with analogous cross section.
- After assigning — in a by no means unique way — permittivity profiles to the individual waveguides, the basis fields are calculated numerically [4, 5, 6]; for fixed core dimensions this is necessary only once.
- With the basis mode profiles translated over the cross section plane according to the actual (z-dependent) core position, local coupling matrices can be computed that establish the local coupled mode equations. The implemented expressions [7] are justified as an approximate description of longitudinally constant structures only.
- For (slowly) longitudinally varying structures, one can expect that these coupled mode equations still yield reasonable approximations, provided that the longitudinal variation of the coupling matrices is taken into account. The coupled mode equations constitute a linear system of ordinary differential equation with — due to the varying waveguide distance — nonconstant coefficients. That system is integrated numerically by means of a standard Runge-Kutta algorithm [8].
- The solution of the coupled mode equations establish the scattering matrix of the directional coupler element, the coefficients of which serve as direct input to the expressions in Ref. [2].

As outlined in the next sections, these steps provide a computationally relatively cheap means for an approximate assessment of the coupler performance, based on existing implementations of the mode solver and the coupled mode approach.

2 Basis fields and supermodes

Specialize to a coupler cross section as shown in Figure 2. The port waveguide with core width s, thickness v, and refractive index n_g is embedded in a medium with refractive index n_b, buried at a distance b below the surface $x = 0$ of that medium. The cavity strip of width w and thickness t with refractive index n_r is placed on top of the surface, covered by a material with refractive index n_a. The horizontal position of the port waveguide is defined by the y-coordinate g (positive or negative values are to be considered) of the core center. p is the horizontal, z-dependent displacement of the ring rim as introduced in Figure 1.

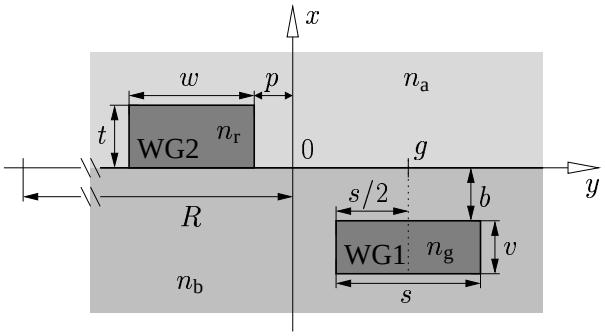

Figure 2: Cross section view of the coupler structure. $p(z)$ is the local lateral displacement of the outer flank of the ring waveguide from the position $p(0) = 0$ at $z = 0$.

Omitting the port core (WG1) to define the refractive index profile for the isolated ring waveguide (WG2) seems to be a natural choice. Hence the basis mode associated with the ring is calculated for a raised strip of width w, thickness t, refractive index n_r, supported by a material with refractive index n_b, and covered by a medium with refractive index n_a.

When defining the isolated port waveguide, the cavity core is to be removed. Mainly for reasons of convenience we also remove the cladding medium, extending the lower background material to the region $x > 0$. To some degree this is justified, because for the interesting configurations of coupled, overlapping fields the port mode profile will sense mainly the presence of the ring core for $x > 0$, not the lower refractive index cladding region. Defining the port waveguide profile as a rectangular core of width s, thickness v, refractive index n_g, embedded in a medium with refractive index n_b, allows to use the port mode profile as a basis field for arbitrary values of the burying depth b.

The first rows of Figures 3, 4 show example profiles for the basis fields with the parameters of Table 1, calculated by the semivectorial version of a semianalytic technique as described in Refs. [4, 5, 6]. For TE polarized light, the two isolated waveguides are almost phase matched with an effective refractive index of 1.500 at a vacuum wavelength $\lambda = 1.55\,\mu$m. The fields are internally represented by analytic functions which are not restricted to a spatial computational window, hence they are well suited for further processing in the framework of the coupled mode theory.

s	$2.0\,\mu$m	n_b	1.45	(SiO_2)
v	$0.14\,\mu$m	n_g	1.98	(Si_3N_4)
w	$2.75\,\mu$m	n_r	1.596	(PMMA–DR1 @ $1.55\,\mu$m)
t	$1.0\,\mu$m	n_a	1.0	
λ	$1.55\,\mu$m	b		$\in [0.5, 2.5]\,\mu$m
R	$100\,\mu$m	g		$\in [-3.0, 4.0]\,\mu$m

Table 1: Simulation parameters that lead to the results of Figures 3–7, for coupler structures according to Figures 1, 2.

The theory as formulated in Ref. [7] leads to coupled mode equations in matrix form

$$\mathsf{S}\,\partial_z \boldsymbol{C} = -\mathrm{i}(\mathsf{B} + \mathsf{K})\,\boldsymbol{C} \tag{1}$$

for the vector $\boldsymbol{C} = (C_1, C_2)^\mathsf{T}$ of z-dependent mode amplitudes, where indices 1 and 2 refer to the port- and cavity modes, respectively. See the reference for the precise definition of the 2×2 coupling matrices S, B, K and for their specific properties.

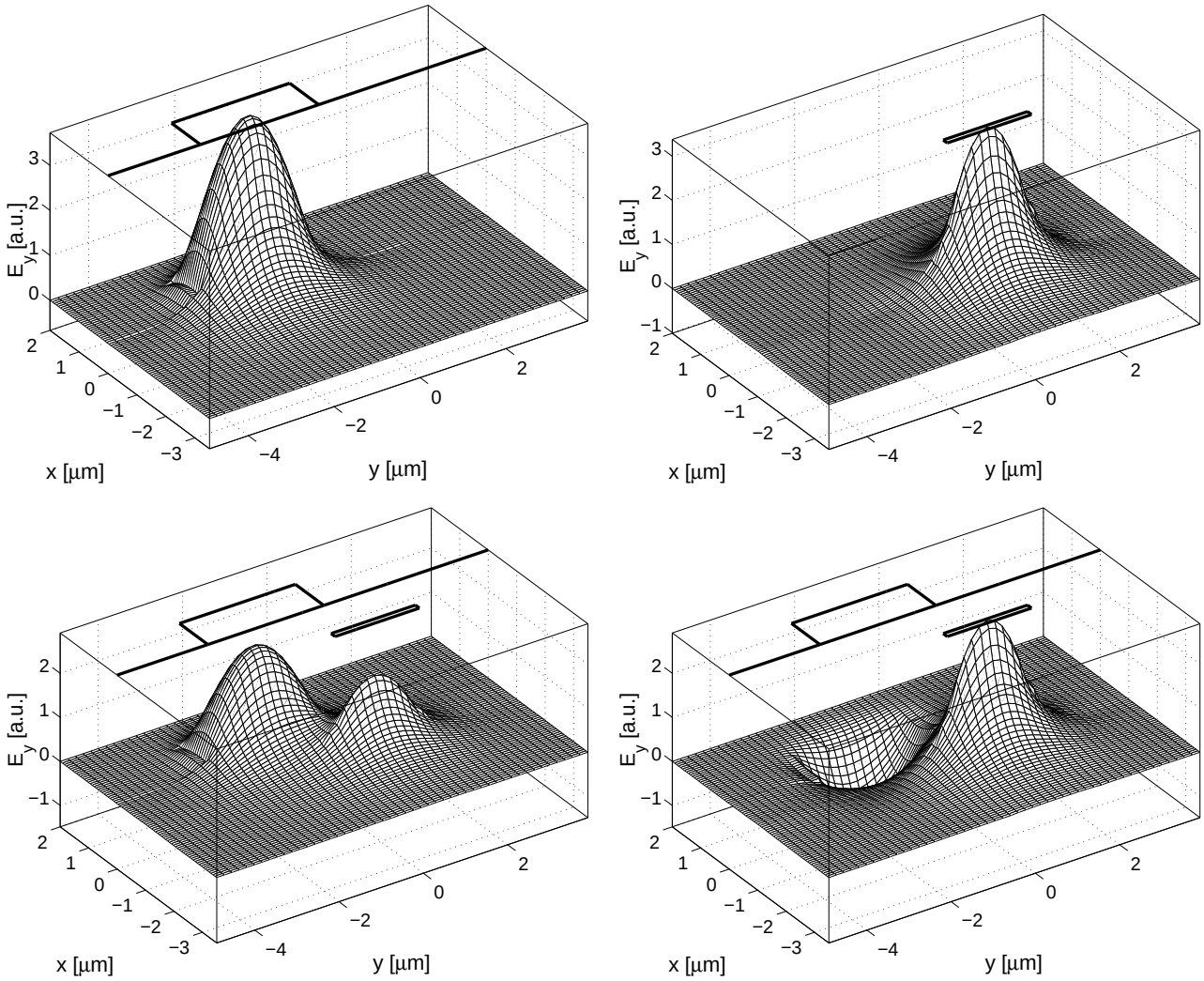

Figure 3: Basis mode profiles of the ring and of the port waveguide (top row), and the local CMT-supermode profiles (bottom) at $z = 0$ ($p = 0$), for parameters as given in Table 1, with $g = 0.5\ \mu$m and $b = 1.0\ \mu$m. The plots show the (real) lateral electric component E_y of the TE polarized modes. The relative amplitudes of the basis fields in the supermodes are given by vectors $(0.48, 0.82)$ (left, symmetric-like field) and $(0.88, -0.58)$ (right, antisymmetric-like field).

Assuming for the moment that the structure is longitudinally invariant, Eq. (1) is readily solved by an ansatz of so-called supermodes, as outlined in Ref. [7]. The corresponding field profiles, shown in the bottom rows of Figures 3, 4, can be viewed as approximations to the two guided TE modes of the total, composite waveguide that includes both cores. The corresponding propagation constants β_s and β_a define a coupling length or half beat length $L_\mathrm{c} = \pi/(\beta_\mathrm{s} - \beta_\mathrm{a})$ that can give a first hint whether a significant power transfer can be expected from a limited coupling region of this shape. Specifically, for the configuration of Figure 3 with larger core distance, thus with weaker coupling, this length evaluates to $L_\mathrm{c} = 102\ \mu$m. The configuration with aligned core centers of Figure 4 leads to stronger coupling with a shorter beat length $L_\mathrm{c} = 33\ \mu$m.

The maximum amount of power that can be transferred between the participating cores is indicated by the balance of the relative contributions of the basis modes to the supermode fields. For the configuration with misaligned cores one finds supermodes where the absolute values of the port- and cavity mode amplitudes deviate considerably (though one can still recognize a symmetry property, according to the signs of the individual amplitudes), in contrast to the strongly coupled structure, where the individual amplitudes are properly balanced in both supermode vectors. Hence for a (still longitudinally invariant) coupler with the parameters of Figure 4 of length L_c one can expect an almost complete power transfer, while for the shifted cores one observes not only a coupling length that is three times as long, but also a considerably reduced upper limit for the relative amount of optical power that is exchanged between the cores.

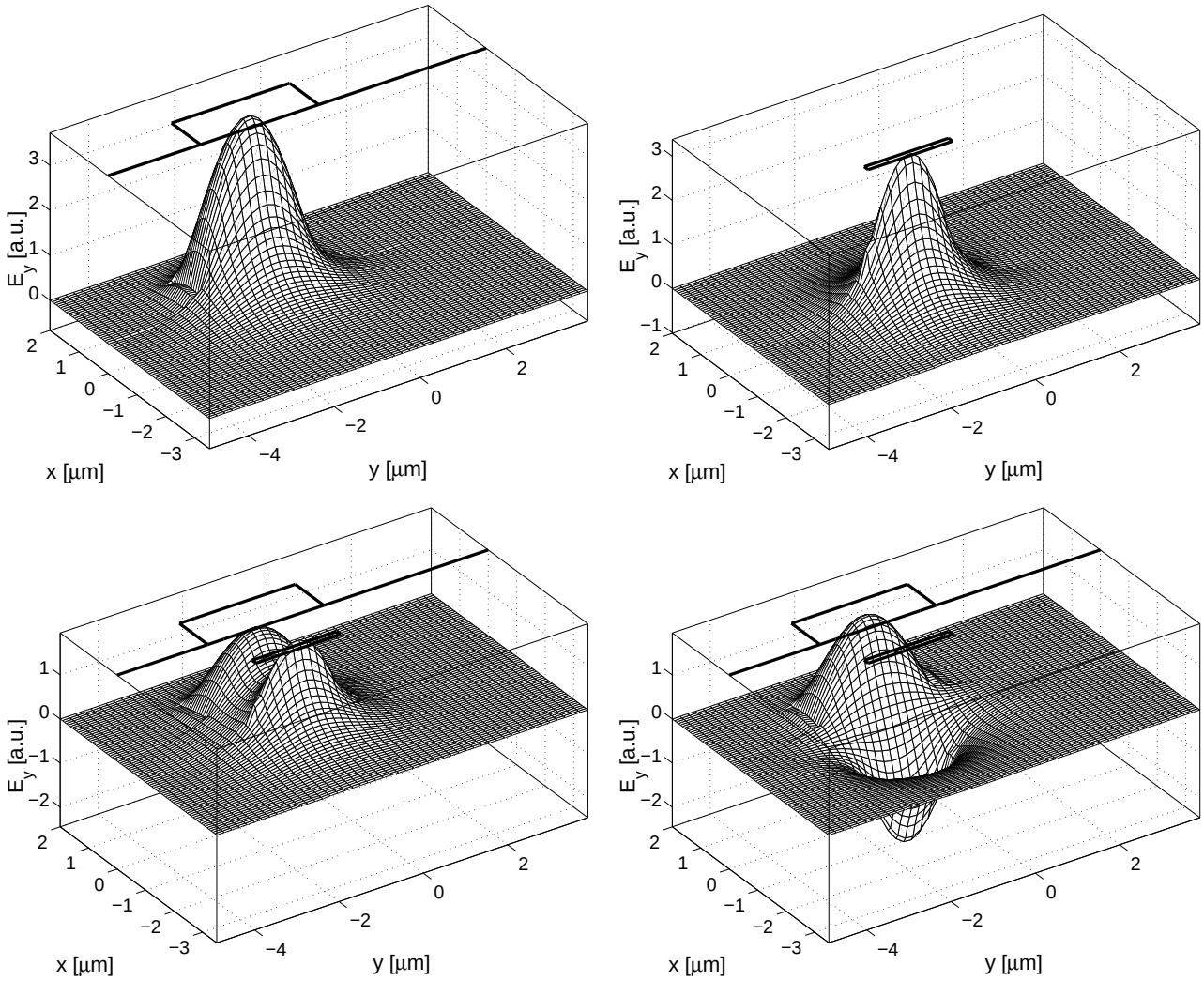

Figure 4: Basis mode profiles of the ring and of the port waveguide (top row), and the local CMT-supermode profiles at $z = 0$ ($p = 0$), for parameters as given in Table 1, with $g = -w/2$ and $b = 1.0\,\mu$m. The plots show the (real) lateral electric component E_y of the TE polarized modes. The relative amplitudes of the basis fields in the supermodes are given by vectors $(0.62, 0.62)$ (left, symmetric-like field) and $(-0.85, 0.85)$ (right, antisymmetric-like field).

This finding is different from what is usually observed for symmetrical couplers with two identical cores, where enlarging the core distance merely leads to an increased beat length, while still complete power transfer can be realized. Closer examination of the coupled mode equation reveals that the upper limit of the power conversion is determined by a phase matching condition that involves the propagation constants of the basis modes, shifted by a small amount due to the presence of the second core. While for a symmetrical coupler both individual effective indices are perturbed by the same amount, this is no longer true for a nonsymmetrical arrangement with different core cross sections. Aiming at a nonsymmetric coupler design with a high maximum power transfer, one has to achieve phase matching of the basis fields including the phase shifts that are induced by the composite refractive index profile.

For the configuration of Figure 3, the larger phase mismatch is mainly caused by the presence of the low index cladding medium that lowers the propagation constant of the port waveguide mode. For the modes of Figure 4, the port waveguide mode senses the cavity core rather than the cladding, hence the effective mode indices remain balanced.

3 Mode amplitude evolution

If applied to the moderately longitudinally varying structure of Figure 1 (with large R), the matrices in Eq. (1) must be assumed to depend on z as well as the mode amplitudes $\boldsymbol{C}$. An ordinary linear differential equation

$$\partial_z \boldsymbol{C}(z) = -\mathrm{i}\mathsf{S}^{-1}(z)\,(\mathsf{B}(z)+\mathsf{K}(z))\,\boldsymbol{C}(z) \tag{2}$$

is to be solved, given initial values $\boldsymbol{C}(-Z)$.

So far the mode amplitudes C_j include the rapid phase oscillation with z according to the propagation constants of the ring and port modes. To avoid having to follow these oscillations numerically, one can split off the rapidly varying part by defining

$$\boldsymbol{A}(z) = \exp(\mathrm{i}\hat{\beta}z)\,\boldsymbol{C}(z), \tag{3}$$

where $\hat{\beta}$ is the average of the propagation constants of the two basis modes. If these are similar, the quantity $\boldsymbol{A}$ can be expected to be much slowlier varying than $\boldsymbol{C}$, allowing for a larger stepsize in a numerical integration procedure. $\boldsymbol{A}$ satisfies the equation

$$\partial_z \boldsymbol{A}(z) = \mathsf{M}(z)\,\boldsymbol{A}(z) \quad \text{with} \quad \mathsf{M}(z) = \mathrm{i}\hat{\beta}\,1 - \mathrm{i}\mathsf{S}^{-1}(z)\,(\mathsf{B}(z)+\mathsf{K}(z))\,. \tag{4}$$

Assuming that $\mathsf{M}_j = \mathsf{M}(z_j)$ is sampled at $N+1$ equidistant points $z_j = -Z + jh$, for $j = 0,\ldots,N$, with $h = 2Z/N$, and additionally at intermediate points $\mathsf{M}_{j+} = \mathsf{M}(z_j + h/2)$, a fourth order Runge-Kutta integration routine [8] can be formulated directly for the propagation matrices T_j that relate the discretized amplitudes $\boldsymbol{A}_j = \boldsymbol{A}(z_j)$ to the initial values $\boldsymbol{A}_0 = \boldsymbol{A}(-Z)$. With $\mathsf{T}_0 = 1$, the propagation matrices are computed stepwise (with matrices N_m being redefined in each step) according to

$$\begin{array}{lcl} \mathsf{N}_1 & = & h\mathsf{M}_j \\ \mathsf{N}_2 & = & h\mathsf{M}_{j+}(1+\mathsf{N}_1/2) \\ \mathsf{N}_3 & = & h\mathsf{M}_{j+}(1+\mathsf{N}_2/2) \\ \mathsf{N}_4 & = & h\mathsf{M}_{j+1}(1+\mathsf{N}_3) \\ \mathsf{T}_{j+1} & = & (1+\mathsf{N}_1/6+\mathsf{N}_2/3+\mathsf{N}_3/3+\mathsf{N}_4/6)\mathsf{T}_j\,, \end{array} \tag{5}$$

such that $\boldsymbol{A}_j = \mathsf{T}_j\boldsymbol{A}_0$ and $\boldsymbol{C}(z_j) = \exp(-\mathrm{i}\hat{\beta}z_j)\,\boldsymbol{A}_j$.

Figure 5 shows plots of amplitude evolutions that are computed in this way, uniformly for integration parameters $N = 40$ and $Z = 40\,\mu$m. On the displayed scale, the curves are stable with respect to both N and Z. Modeling an excitation in the port waveguide, the computations start with $\boldsymbol{C}(0) = (1,0)^{\mathsf{T}}$.

The present approach does not include any loss mechanism, hence the modal powers $|C_1|^2$ and $|C_2|^2$ add always to unity, at least with reasonable accuracy. As expected, the power transfer between the two waveguides starts only after a certain propagation distance, when the cores are sufficiently close, and it levels at the end of what may thus be called the coupling region, with the strongest interaction around $z = 0$. The plots correspond to a configuration, where the core centers are aligned at that position. For a large burying depth, hardly any power transfer is observed. When b is reduced, i.e. the cores are brought vertically closer together, the interaction increases, up to almost total coupling for $b = 1.0\,\mu$m. Reducing b further leads to an even stronger interaction, i.e. to more rapid oscillations of the optical power, but the relative amount of power found in the cavity waveguide at the output port is reduced again, due to the backcoupling into the port core. Thus increasing the interaction strength by reducing the distance between the coupled cores may well lead to a lower total amount of power transfer.

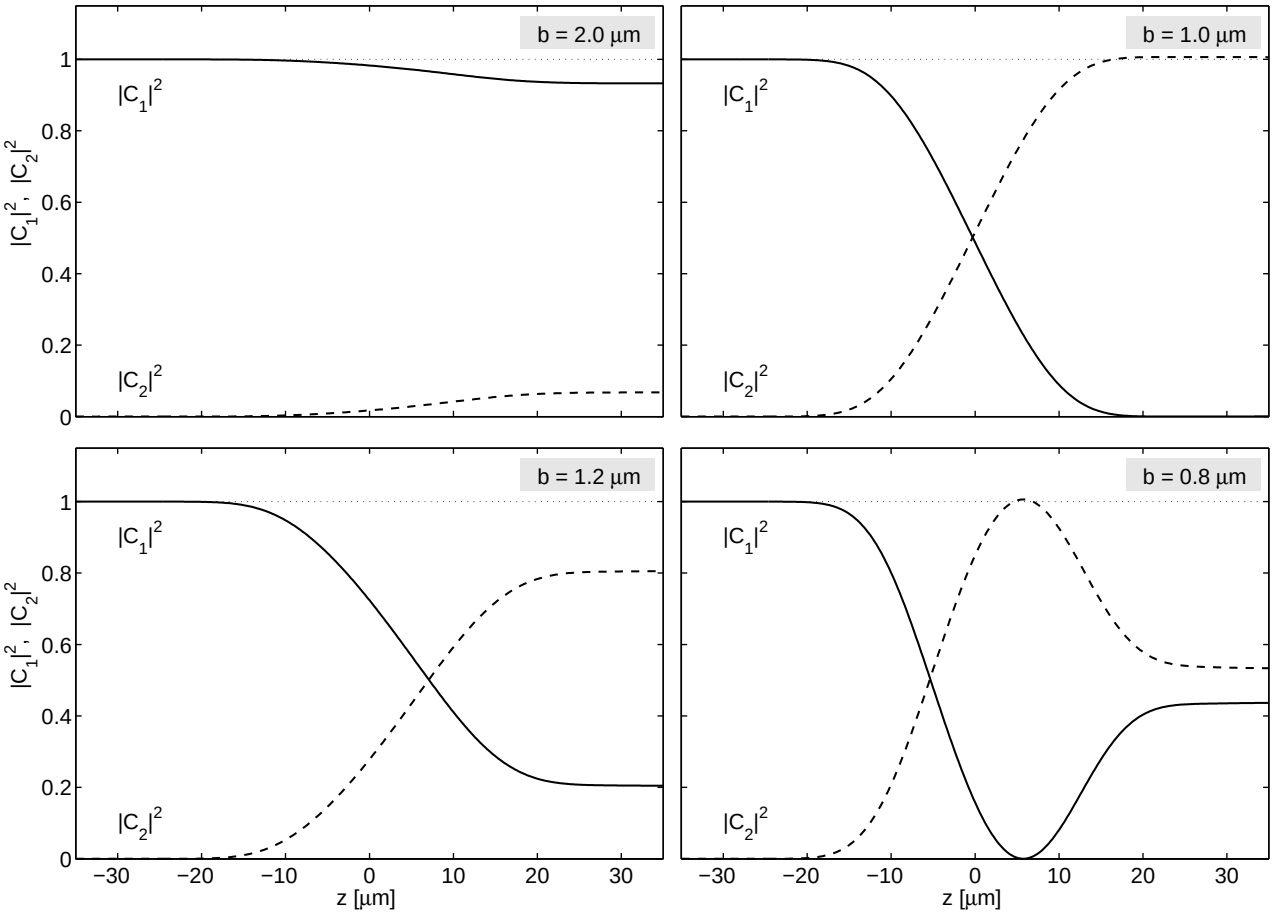

Figure 5: Evolution of the basis mode amplitudes according to the CMT equations, for coupler structures with different burying depth b and parameters as in Table 1, with $g = -w/2$ (centered cores at $z = 0$).

4 Scattering matrices

In the framework of the microresonator model, the coupler operation is described in terms of a 2×2 scattering matrix T that relates the output amplitudes $\boldsymbol{C}(Z) = (B_+, b_+)^\mathsf{T}$ to the the initial values $\boldsymbol{C}(-Z) = (A_+, a_+)^\mathsf{T}$. The numerical integration of the coupled mode equations predicts

$$\boldsymbol{C}(Z) = \mathsf{T}\,\boldsymbol{C}(-Z)\,, \quad \mathsf{T} = \exp(-\mathrm{i}2\hat{\beta}Z)\,\mathsf{T}_N. \tag{6}$$

By virtue of abstract symmetry arguments [9, 2], one expects a relation in the form

$$\begin{pmatrix} B_+ \\ b_+ \end{pmatrix} = \begin{pmatrix} \rho & \kappa \\ \kappa & \tau \end{pmatrix} \begin{pmatrix} A_+ \\ a_+ \end{pmatrix} \tag{7}$$

with a symmetric scattering matrix, where lossless coupler operation requires $|\tau|^2 = |\rho|^2 = 1 - |\kappa|^2$. Though not explicitly incorporated, these properties provide a means to check the consistency of the numerical results. For the given examples, this holds reasonably well, at least on the scale of the shown plots.

Apart from the cavity attenuation constant, the microresonator performance depends on the absolute values of the coupling constant κ and of the coupler transfer coefficient τ (where for the present model $|\tau| = |\rho|$). Figures 6 and 7 show examples for the sometimes quite irregular dependences of these quantities on the parameters g and b that control the horizontal and vertical distance of the cores within the coupler element. These curves should be more or less explainable by a reasoning according to Sections 2, 3.

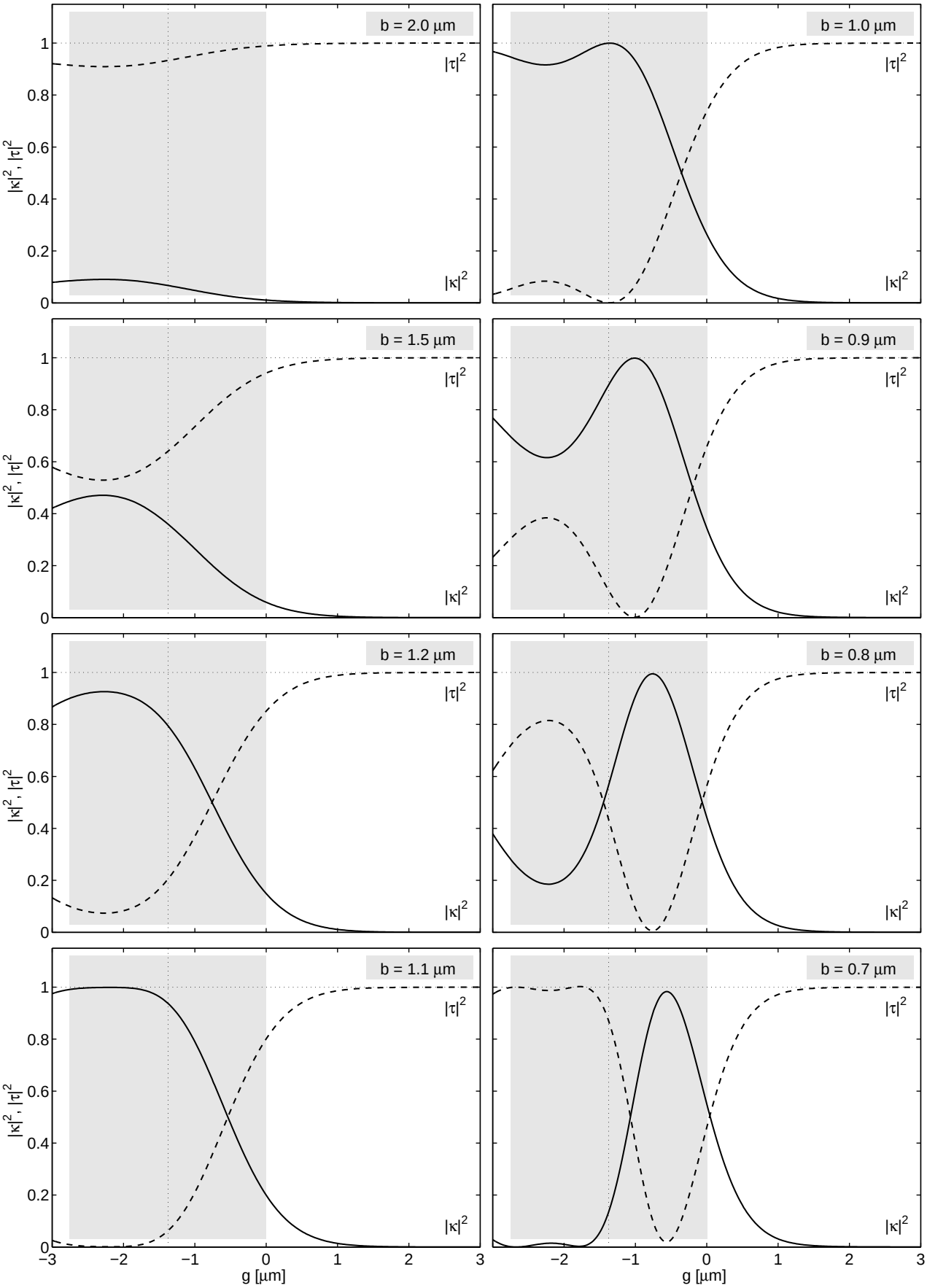

Figure 6: Coupling constant κ and transfer coefficient τ (absolute squares) versus the center position g of the core of the straight waveguide, for different values of the burying depth b. Other parameters are as given in Table 1. The gray regions indicate the extension of the ring core at $z = 0$.

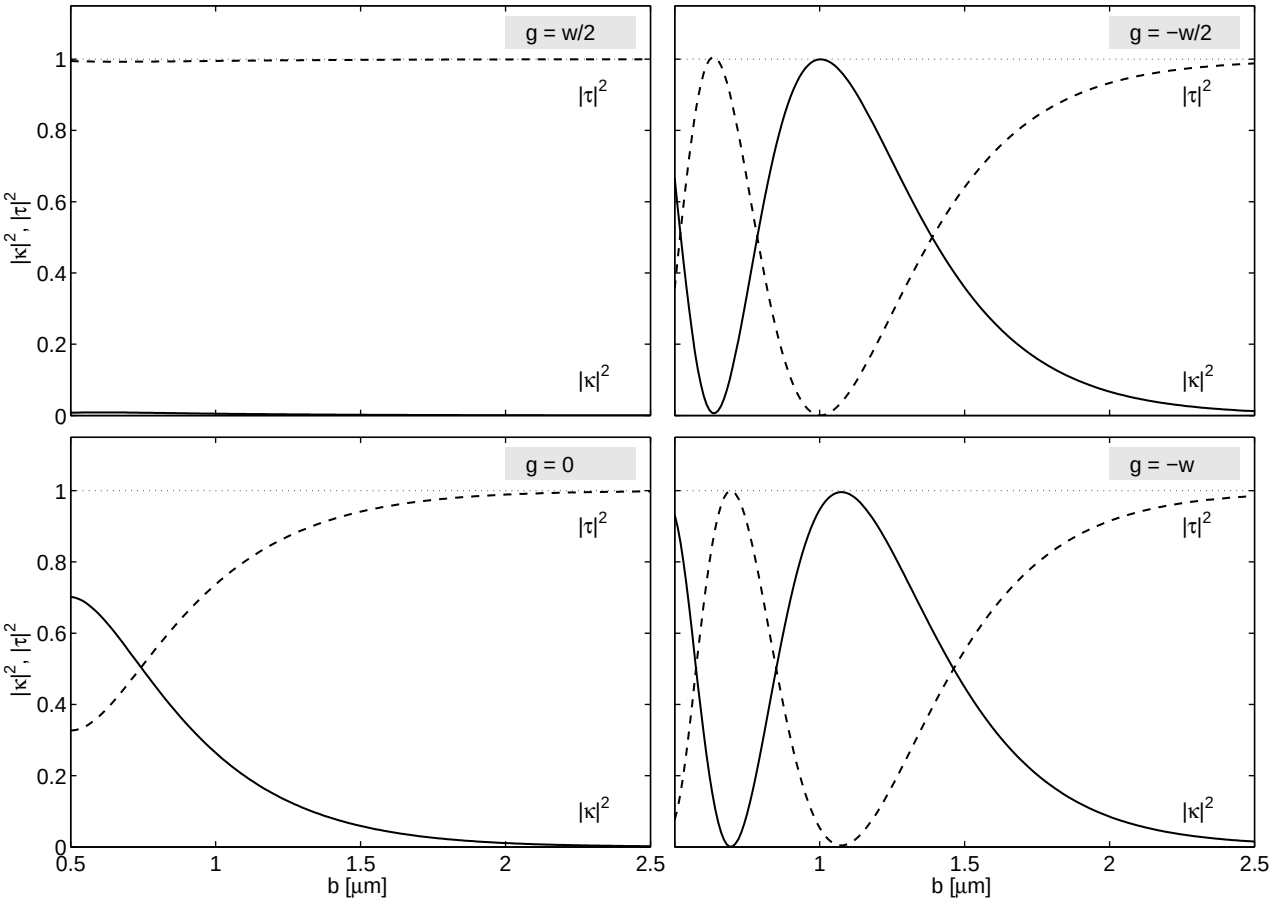

Figure 7: Coupling constant κ and transfer coefficient τ (absolute squares) versus the burying depth b of the core of the straight waveguide, for different values of its center position g. Other parameters are as given in Table 1.

References

[1] A. Yariv. Universal relations for coupling of optical power between miroresonators and dielectric waveguide. *Electronic Letters*, 36(4):321–322, 2000.

[2] M. Hammer. Standard model for optical ringresonantors. NAIS internal manuscript, 09.2002.

[3] D. G. Hall and B. J. Thompson, editors. *Selected Papers on Coupled-Mode Theory in Guided-Wave Optics*, volume MS 84 of *SPIE Milestone Series*. SPIE Optical Engineering Press, Bellingham, Washington USA, 1993.

[4] M. Lohmeyer. Wave-matching method for mode analysis of dielectric waveguides. *Optical and Quantum Electronics*, 29:907–922, 1997.

[5] M. Lohmeyer. Vectorial wave-matching mode analysis of integrated optical waveguides. *Optical and Quantum Electronics*, 30:385–396, 1998.

[6] WMM mode solver — Numerical simulation of rectangular integrated optical waveguides. `http://www.math.utwente.nl/~hammer/Wmm_Manual/` .

[7] M. Lohmeyer, N. Bahlmann, O. Zhuromskyy, and P. Hertel. Radiatively coupled waveguide polarization splitter simulated by wave-matching based coupled mode theory. *Optical and Quantum Electronics*, 31:877–891, 1999.

[8] W. H. Press, S. A. Teukolsky, W. T. Vetterling, and B. P. Flannery. *Numerical Recipes in C, 2nd ed.* Cambridge University Press, 1992.

[9] C. Vassallo. *Optical Waveguide Concepts*. Elsevier, Amsterdam, 1991.